J. Plasma Phys. (2020), *vol.* 86, 815860301
Published by Cambridge University Press
doi:10.1017/S0022377820000343

Study of intrinsic rotation by the Gyrokinetic Electromagnetic Numerical Experiment code in the Joint Texas Experimental Tokamak

Duoqin Wang[1], Wei Yan[1,†], Zhongyong Chen[1,2], Xin Ye[1], Wei Li[1], Zhiyang Yin[1], Jie Hu[1], Wei Bai[1], Yu Zhong[1] and J-TEXT Team[‡]

[1]International Joint Research Laboratory of Magnetic Confinement Fusion and Plasma Physics, State Key Laboratory of Advanced Electromagnetic Engineering and Technology, School of Electrical and Electronic Engineering, Huazhong University of Science and Technology, Wuhan 430074, People's Republic of China

[2]Chengdu University, 610106, Chengdu, People's Republic of China

(Received 23 December 2019; revised 9 April 2020; accepted 14 April 2020)

The core toroidal plasma intrinsic rotation has been studied by experiments and simulations in the Joint Texas Experimental Tokamak (J-TEXT). The direction of core intrinsic rotation in the J-TEXT plasma is counter-current. As the plasma density ramps up, the rotation velocity increases in the counter-current direction. By comparing four different electron densities, linear local gyrokinetic simulations have been performed by the Gyrokinetic Electromagnetic Numerical Experiment code for the first time on J-TEXT. It is found that the most dominant turbulence is the ion temperature gradient at $0.2a$, where a is the minor radius of the plasma and this is unchanged during the plasma density ramp up. By scanning the radial wave vectors, it is found that the residual stress term reverses from negative to positive when the plasma density exceeds a certain threshold. The pinch term is larger than the residual stress term at all four electron densities, which means that the pinch term is always dominant in the core of a J-TEXT plasma.

Key words: fusion plasma, plasma flows, plasma simulation

1. Introduction

Plasma rotation plays an important role in low confinement mode (L-mode) to high confinement mode (H-mode) transition (Shaing & Crume 1989; Burrell *et al.* 1994; Carraro *et al.* 2000), avoiding or stabilizing magnetohydrodynamic (MHD) instabilities (Bondeson & Ward 1994; Garofalo *et al.* 1999) and suppressing plasma turbulence (Hahm & Burrell 1995; Terry 2000). Plasma can rotate spontaneously without any external momentum sources (Rice *et al.* 1997). Understanding the mechanism of plasma intrinsic rotation is quite important, and there are still some open questions which need to be solved.

† Email address for correspondence: yanwei1090@hust.edu.cn
‡ See the author list of Liang *et al.* (2019)

Generally, core intrinsic rotation has been observed to behave very simply in the H-mode, scaling linearly in the co-current direction with the pedestal ion temperature gradient (Rice *et al.* 2007, 2011*a*). On the other hand, core intrinsic rotation exhibits more complex behaviour in the L-mode. Experiments on Alcator C-mod and tokamak à configuration variable (TCV) (Lee *et al.* 2003; Rice *et al.* 2004; Scarabosio *et al.* 2006; Duval *et al.* 2007, 2008) found that many factors could affect core intrinsic rotation behaviour, such as plasma parameters, magnetic field, plasma configuration and heating method. Early experiments found that plasma core intrinsic rotation behaviour could be related to linear ohmic confinement/saturated ohmic confinement (SOC) transition or dominant plasma turbulence mode transition (Rice *et al.* 2011*b*) but further experiments on AUG and KSTAR showed that plasma rotation could reverse back towards the co-current direction in the SOC regime (McDermott *et al.* 2011, 2014; Na *et al.* 2016). Experiments on AUG (McDermott *et al.* 2014) found that the normalized intrinsic rotation gradient u' depended strongly on local plasma parameters, in particular on the normalized logarithmic electron density gradient R/L_{n_e}. A strong dependence of u' on the effective collision frequency ν_{eff} was clearly observed in the gradient region in KSTAR (Angioni *et al.* 2017). Experimental results on Tore Supra showing toroidal rotation breaking at all radii are in agreement with neoclassical predictions including ripple-induced toroidal friction (Bernardo *et al.* 2015).

Plasma toroidal momentum flux can be decomposed into a diagonal term, pinch term and residual stress which can drive intrinsic rotation (Diamond *et al.* 2013). The diagonal term is proportional to the rotation gradient and the pinch term is proportional to rotation velocity. Residual stress is independent of rotation velocity and gradient, and is closely related to plasma parameters. The symmetry principle limits possible residual stress mechanisms (Parra, Barnes & Peeters 2011; Sugama *et al.* 2011). For local gyrokinetic equations with distribution functions f_S and electric potential ϕ given as functions of local radial position x, binormal position y, parallel position s, parallel velocity $v_\parallel$, magnetic moment μ and time t, if there is an up–down symmetric magnetic geometry, no background toroidal rotation or rotation gradient and no background $E \times B$ shear, then the first-order local equations have the following feature: if specific distribution functions $f_s(x, y, s, v_\parallel, \mu, t)$ and potential $\phi(x, y, s, t)$ solve the local equations, then so do $-f_s(-x, y, -s, -v_\parallel, \mu, t)$ and $-\phi(-x, y, -s, t)$ (Stoltzfus-Dueck 2019). If the first-order momentum fluxes are evaluated with these two different solutions, then equal and opposite values for the radial flux of toroidal angular momentum could be obtained and the momentum flux should vanish. Thus, the breaking of symmetry is responsible for the generation of toroidal rotation (Peeters *et al.* 2011). The most natural mechanism that breaks the symmetry is the presence of toroidal rotation in the plasma. This leads to a pinch term (Hahm *et al.* 2007; Peeters, Angioni & Strintzi 2007; Waltz *et al.* 2007). In the co-moving frame of the plasma, the toroidal rotation leads to additional drifts, connected with the Coriolis and centrifugal inertial forces (Angioni *et al.* 2012). In addition to the equilibrium toroidal rotation, local simulations found that non-zero residual stresses could be driven by $E \times B$ shear (Casson *et al.* 2009), up–down asymmetric magnetic geometry (Camenen *et al.* 2009) and a non-Maxwellian equilibrium (Barnes *et al.* 2013). Global effects such as profile shearing (Camenen *et al.* 2011; Buchholz *et al.* 2014) and the turbulence intensity gradient (Diamond *et al.* 2008; Gürcan *et al.* 2010) and electromagnetic effects such as turbulent acceleration (Wang & Diamond 2013) are proposed to explain the origin of residual stress. Local simulations performed at finite

https://doi.org/10.1017/S0022377820000343 Published online by Cambridge University Press

radial wave vector showed that the profile shearing effect could induce residual stress and was mainly due to the antisymmetric radial component of the magnetic drift (Camenen *et al.* 2011). This symmetry breaking mechanism can have comparable contributions from the radial variation of density and temperature and of their gradients. Note that the profile shearing effect is related to the global model, several efforts have focused on developing local mock-ups of the global, radial profile shear effects, typically based on some extension of the ballooning formalism for high $k_\perp$ instabilities (Connor, Hastie & Taylor 1979; Dewar & Glasser 1983; Stoltzfus-Dueck 2019). In local simulations the profile shear effect can be replaced by the poloidal tilt angle θ which is the tilt of maximum turbulence intensity at the outboard midplane and can be related to ballooning angle θ_0. Shifting each of the elements in radial wavenumber k_x by some non-zero values rotates the mode structure in θ and stations it away from the low field side midplane (Singh *et al.* 2014). Simulations performed at different magnetic shear showed a new symmetry breaking mechanism in residual stress generation which was related to the turbulence intensity gradient effect and became dominant at weak magnetic shear (Lu *et al.* 2015). Simulations using non-Maxwellian equilibrium showed that the radial flux of toroidal angular momentum had a strong dependence on collisionality (Barnes *et al.* 2013). The flux reversed direction from radial inward to outward as collisionality increased. A novel one-dimensional model which captures the collisionality dependence of the radial transport of toroidal angular momentum due to the effect of neoclassical flows on turbulent fluctuations had been compared to MAST experimental results (Hillesheim *et al.* 2015). This model showed that local intrinsic momentum flux changes sign close to the normalized collisionality $v_* \approx 1$ and is independent of v_* at high and low v_*. Simulations performed on KSTAR showed that the neoclassical equilibrium effect could not match the experimental results and the profile shearing effect well reproduced the experimental rotation gradient u' of both the gradient region and the anchor point (Na *et al.* 2016). Simulations performed on ohmic L-mode AUG plasmas showed that the symmetry breaking effects due to neoclassical background flows could produce significant toroidal momentum transport but still were not sufficient to explain the maximum flow gradients observed in AUG (Hornsby *et al.* 2017). The flow gradient was closely related to density profile curvature and the profile shearing effect is the dominant mechanism in producing a finite parallel wavenumber in AUG plasmas (Hornsby *et al.* 2018).

In this paper, we focus on the influence of the poloidal tilt on the momentum transport in the plasma core ($\rho = r/a$, where $r = 0$ denotes the magnetic axis of the plasma, and a is the minor radius of the plasma). The rest of the paper is organized as follows. In § 2, the descriptions of tangential X-ray imaging crystal spectrometer (XICS) systems and gyrokinetic simulations used for this study are given. In § 3, the measurements of the core toroidal plasma rotation and the growth rate/frequency spectra using GENE (Jenko *et al.* 2000; Dannert & Jenko 2005; Görler *et al.* 2014) in a J-TEXT ohmic plasma are presented. The effect of poloidal tilt on the core toroidal plasma rotation are also compared with the measurements. The summary is given in § 4.

2. Experimental and simulated set-up

The J-TEXT tokamak is a conventional iron core tokamak, operated at a major radius $R_0 = 1.05$ m, minor radius $a = 25$–29 cm with a movable titanium-carbide-coated graphite limiter (Liang *et al.* 2019). The main parameters of the typical

https://doi.org/10.1017/S0022377820000343 Published online by Cambridge University Press

Typical simulation parameters	
Number of grid points in the radial direction, nx0	15
Number of Fourier modes in the bi-normal direction, nky0	1
Number of grid points in the parallel direction, nz0	32
Number of grid points in the parallel velocity direction, nv0	48
Number of grid points in the magnetic moment direction, nw0	16
Plasma beta	−1
Collision operator	Landau
Normalized collision frequency	−1
Effective ion charge, z_{eff}	1
$E \times B$ shearing rate, ExBrate	0.01
Parallel flow shear, pfsrate	−1
Numerical dissipation in the parallel direction	−1
The sign of the plasma current/toroidal magnetic field component	−1
The sign of the toroidal angular velocity	1

TABLE 1. Typical simulation parameters used in all the following simulations.

J-TEXT discharges are as follows: toroidal field $B_T = 1.0\sim2.2$ T, plasma current $I_p = 80\sim220$ kA, plasma density $n_e = (1\sim6) \times 10^{19}$ m^{-3}. In this paper, the parameters of the experiment are: $B_T = 1.8$ T, $I_p = 180$ kA, $n_e = (2\sim4) \times 10^{19}$ m^{-3}, the edge safety factor $q_a = 3.3$. The tangential X-ray imaging crystal spectrometer, based on a Pilatus detector with a 500 Hz frame rate, has been upgraded to measure the rotation velocity of helium-like argon (Ar XVII) and electron/ion temperature in the core region in the J-TEXT tokamak (Yan *et al.* 2014, 2018). The maximum temporal resolution is 2 ms and spatial resolution is approximately 1.8 cm in $\rho = 0\sim0.4$ along the vertical direction. Due to the small core ion temperature gradient, the main ion rotation velocity and the argon impurity rotation velocity are almost equal. In this paper, the positive value and negative value of toroidal rotation velocity represent the co-current direction and counter-current direction, respectively. The electron density and safety factor profile are measured by POLARIS which is a multi-chord interferometer– polarimeter diagnostic (Zhuang *et al.* 2013).

To study the influence of the poloidal tilt on the momentum transport in the plasma core, the gyro-kinetic plasma microturbulence code GENE is used. GENE is an open source plasma microturbulence code which can be used to efficiently compute gyroradius-scale fluctuations and the resulting transport coefficients in magnetized fusion plasmas (Jenko & GENE development team 2019). It solves the δf-split gyrokinetic system of equations using a Eulerian approach (fixed grid) in five-dimensional phase space.

All simulations are linear and the simulation positions are $0.2a$, $0.3a$ and $0.4a$. The magnetic surface equilibrium inversion in J-TEXT is currently unavailable. Thus, simulations run with a circular geometry, which is a reasonable approximation in the core of the J-TEXT ohmic plasma. Only one ion species, hydrogen, is considered and electrons are treated as kinetic in all the following simulations. The typical simulation parameters used in all simulations are shown in table 1.

The values of the plasma beta and normalized collision frequency are −1, which means their actual values are calculated by GENE automatically, and a Landau–Boltzmann collision operator is used. In GENE, the Landau–Boltzmann

https://doi.org/10.1017/S0022377820000343 Published online by Cambridge University Press

collision operator is

$$C(F_\sigma, F_{\sigma'}) = \frac{\partial}{\partial \boldsymbol{v}} \cdot \left(\boldsymbol{D} \cdot \frac{\partial}{\partial \boldsymbol{v}} - \boldsymbol{R} \right) F_\sigma, \tag{2.1}$$

where $\boldsymbol{D}$ denotes a diffusion tensor and $\boldsymbol{R}$ is the dynamical friction. Further details can be found in Görler *et al.* (2011). The value of numerical dissipation in the parallel direction is set to -1, which mimics third-order upwind dissipation. The value of adapt_lx is set to true, which maximizes the number of poloidal connections for a given nx0, and means that only one linearly independent mode is considered (GENE development team 2018). ExBrate is the parameter that defines a radially constant $E \times B$ shearing rate. This parameter is given in normalized units by

$$\text{ExBrate} = -\frac{\psi_0}{q_0} \frac{\partial \Omega_{\text{tor}}}{\partial \psi} \frac{R_0}{c_{\text{ref}}}, \tag{2.2}$$

where $\psi = r/R_0$ and ψ_0 are the radial coordinate and reference flux surface position, respectively, q_0 is the safety factor, $\partial \Omega_{\text{tor}}/\partial \psi$ is the radial derivative of the toroidal angular velocity Ω_{tor} and $c_{\text{ref}} = \sqrt{T_i/m_i}$ is the reference velocity. The GENE input parameter pfsrate is the parameter that defines the shearing rate to model the parallel flow shear drive that appears due to toroidal rotation. Its value is set to -1 so that the parallel flow shear equals ExBrate as given for a purely toroidal flow (GENE development team 2018). When nx0, nz0, nv0 and nw0 are larger than 15, 32, 48 and 16 respectively, the growth rate and mode frequency change no more than 5 %. The simulation grid resolution check is shown in figure 1. The plasma parameters used in these simulations are selected from the first density point in § 3. Note that the plasma beta is small in the J-TEXT tokamak, a small but finite beta value can help to increase the time step significantly. The direction of the plasma current and toroidal magnetic field component is counter-clockwise (viewed from above) in J-TEXT, and the direction of toroidal rotation velocity is usually clockwise.

3. Linear local simulations

3.1. *Experiment results*

The parameters during the density ramping-up phase of an ohmic heated discharge (shot number 1057259) are shown in figure 2. The plasma current is $I_p = 180$ kA and the maximum central line average density has reached approximately $n_e = 4 \times 10^{19}$ m^{-3}, and toroidal magnetic field is $B_T = 1.8$ T. Overall, as the plasma line average density ramped from 2×10^{19} m^{-3} to 4×10^{19} m^{-3}, the plasma rotation increased toward counter-current direction and finally reached approximately -50 km s^{-1}. This trend is the same as that on AUG and KSTAR, however, the direction of plasma rotation is co-current at low density and the plasma rotation increases toward the co-current direction as the density increases when the density exceeds a certain threshold on AUG and KSTAR (McDermott *et al.* 2014; Na *et al.* 2016). This phenomenon is currently not observed in J-TEXT. The change in the plasma toroidal rotation can be divided into three stages. First, the change of the plasma toroidal rotation was not large from 0.1 s to 0.24 s as the plasma density changed little. Next, when the plasma density ramped up rapidly, the plasma rotation increased toward the counter-current direction from -36 km s^{-1} to -50 km s^{-1} in the period 0.24 s to 0.32 s. Finally, as the density increased from 3×10^{19} m^{-3} to 4×10^{19} m^{-3}, the rotation kept at a stable velocity. According to the experimental results, four density points are selected for simulation in the density ramping up stage.

https://doi.org/10.1017/S0022377820000343 Published online by Cambridge University Press

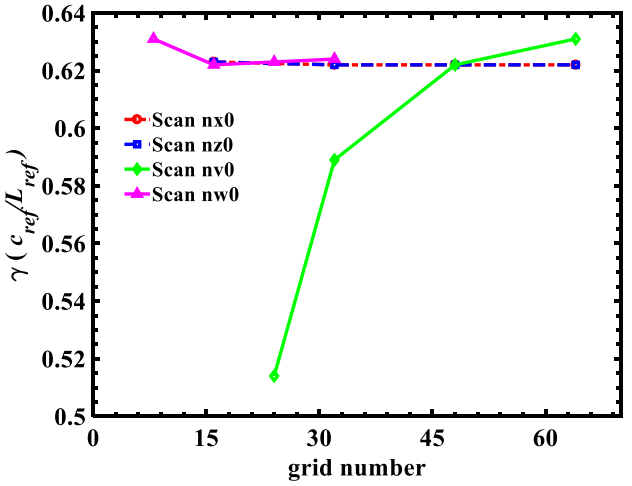

FIGURE 1. The simulation grid resolution check for the first density point simulation in § 3. These simulations do not include a toroidal rotation/toroidal rotation gradient and $k_y\rho_{\mathrm{ref}}$ is set to 0.485. In all the following simulations nx0, nz0, nv0 and nw0 are chosen to be 15, 32, 48 and 16, respectively.

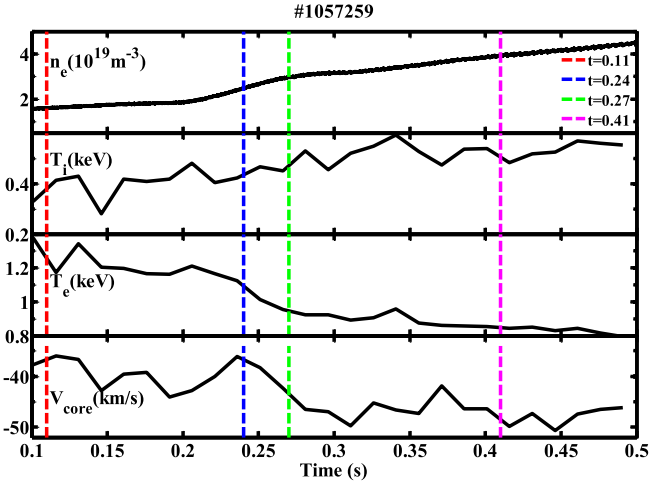

FIGURE 2. Typical discharge waveforms of experiment in shot no. 1057259. From top to bottom are plasma density, ion temperature, electron temperature and toroidal core rotation velocity. Four time points are selected for simulations which are 0.11 s, 0.24 s, 0.27 s and 0.41 s and are represented by red, blue, green and pink dashed lines, respectively.

The four density points are 2.25×10^{19} m^{-3} when the plasma rotation velocity was approximately -40 km s^{-1}, 3.46×10^{19} m^{-3} and 4.33×10^{19} m^{-3} when the plasma rotation started to increase toward the counter-current direction and 6.04×10^{19} m^{-3} when the plasma rotation no longer increased. The profiles of some key plasma parameters of shot no. 1057259, including plasma density, ion temperature, electron temperature and their normalized characteristic length reciprocals, are also shown in figure 3, where n_{ref} referred to the plasma density value of each position, and T_{ref} was ion temperature value of each position.

https://doi.org/10.1017/S0022377820000343 Published online by Cambridge University Press

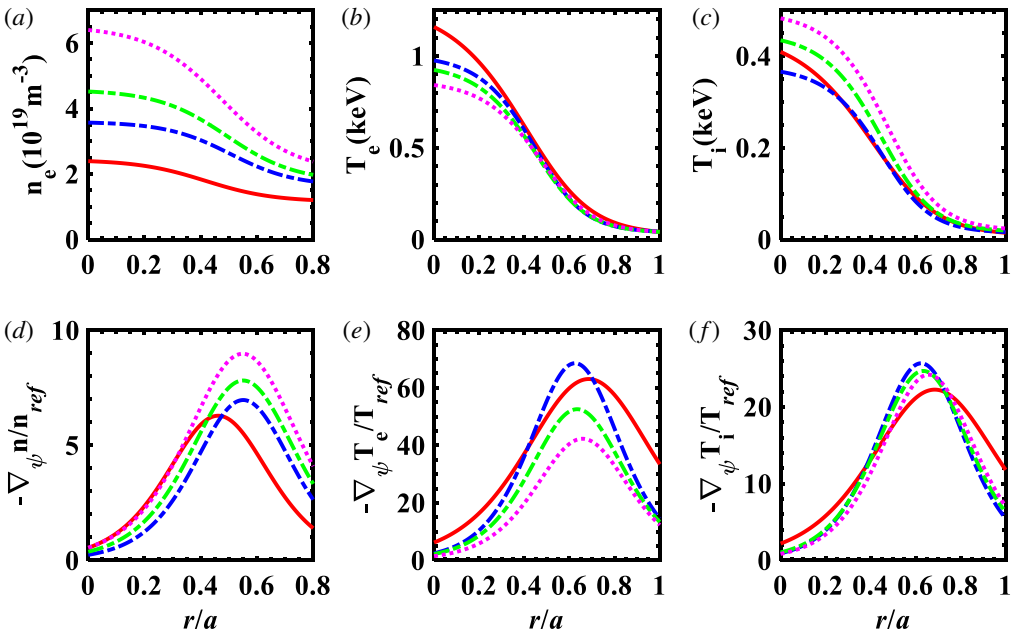

FIGURE 3. Profiles of plasma parameters at four time points. (*a–f*) Plasma density, electron temperature, ion temperature, normalized gradient of plasma density, normalized gradient of electron temperature and normalized gradient of ion temperature. ψ is the ratio of small radius r to large radius R. Red, blue, green and pink colours represent 0.11 s, 0.24 s, 0.27 s and 0.41 s, respectively.

3.2. *Simulation results*

In this section, the local linear version of the gyrokinetic code GENE is used to investigate the change of the turbulent dominant mode during the plasma density ramping up and the impact of finite poloidal tilt on momentum transport in J-TEXT plasmas. Input data used for simulations came from experimental measurements which have been described above. Some key plasma parameters at four time points are shown in table 2, where v_{eff} is the effective collision frequency. The toroidal rotation velocities at four time points at $0.2a$ (0.11 s, 0.24 s, 0.27 s and 0.41 s) are -36 km s^{-1}, -36 km s^{-1}, -42 km s^{-1} and -50 km s^{-1} respectively. Due to the limitation of the experimental conditions, XICS can only measure the core rotation velocity at present, and the measurement error of other positions is quite large. For simplicity, the toroidal rotation velocities at $0.3a$ and $0.4a$ are the same as at $0.2a$. To calculate the Prandtl number, a realistic toroidal rotation gradient, which has been described in § 2, was added to the simulations. The simulations at each time point are divided into three cases: without toroidal rotation V_φ and toroidal rotation gradient V'_φ, only with toroidal rotation and only with toroidal rotation gradient.

The growth rate/frequency spectra at four electron density points at $0.2a$ are shown in figure 4. The case of considering toroidal rotation is represented by blue dots, and red dots mean no rotation. As shown in figure 4, toroidal rotation has little effect on the growth rate/frequency spectra, which means turbulence characteristics have not changed. In GENE, positive frequencies indicate an ion diamagnetic drift, and negative frequencies indicate an electron diamagnetic drift. So positive frequencies mean an

https://doi.org/10.1017/S0022377820000343 Published online by Cambridge University Press

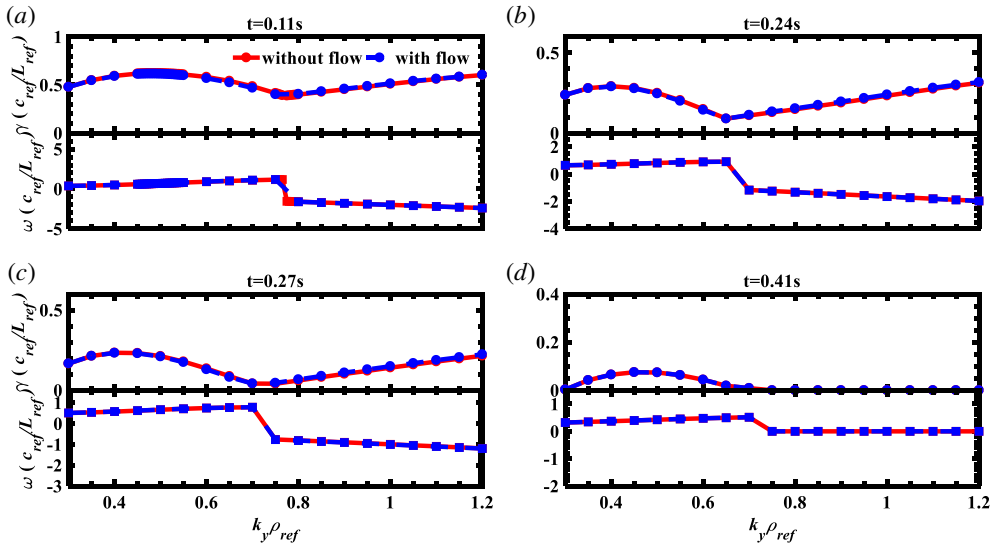

FIGURE 4. The growth rate/frequency spectra at four density points at $0.2a$. Red dots indicate that there is no rotation, and blue dots indicate that rotation is added.

t/s	0.11	0.24	0.27	0.41
$\psi = r/R_0$	0.049	0.049	0.049	0.049
q	0.98	0.99	0.98	0.98
s	0.096	0.089	0.081	0.077
n_e/m^{-3}	2.25×10^{19}	3.46×10^{19}	4.33×10^{19}	6.04×10^{19}
$-\nabla_\psi n_e/n_e$	2.33	1.22	1.67	2.21
T_i/keV	0.34	0.33	0.39	0.44
T_e/T_i	2.83	2.67	2.13	1.75
$\eta_i = \mathrm{dIn}(T_i)/\mathrm{dIn}(n)$	2.47	3.15	2.40	1.50
$\nu_{\mathrm{eff}} = 0.1 Z_{\mathrm{eff}} R_0 n_e T_e^{-2}$	0.26	0.47	0.66	1.07

TABLE 2. Some key plasma parameters at four density points at $0.2a$.

ion temperature gradient mode (ITG) and negative frequencies mean trapped electron modes (TEM) when $k_y\rho_{\mathrm{ref}} \sim 1$. In figure 4, the first three density points have positive and negative mode frequencies, which indicates that the turbulent modes include ITG and TEM, but the maximum growth rate corresponding to the positive mode frequency is greater than the one corresponding to the negative mode frequency, so ITG is the dominant turbulent mode at the first three density points. For the fourth density point, the mode frequency is always greater than zero, so the dominant turbulent mode is ITG. As the plasma density is ramped up, the normalized gradient of plasma density and ion/electron temperature decrease gradually, and the maximum growth rate also drops. The maximum growth rate and its corresponding mode frequency and $k_y\rho_{\mathrm{ref}}$ in each simulation are shown in table 3. The growth rate spectra of four density points at $0.2a$, $0.3a$ and $0.4a$ are shown in figure 5. The growth rate has been multiplied by the sign of mode frequency, therefore a positive growth rate means the turbulent mode is ITG and negative growth rate means TEM. The zero-value boundaries of the four

https://doi.org/10.1017/S0022377820000343 Published online by Cambridge University Press

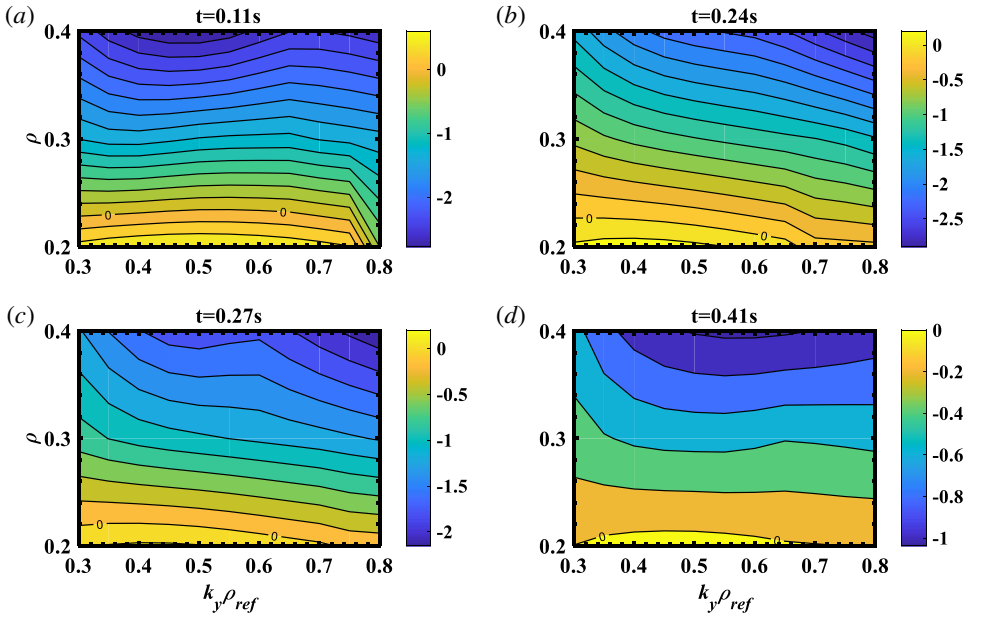

FIGURE 5. Evolution of growth rate at four density points at $0.2a$, $0.3a$ and $0.4a$. The growth rate has been multiplied by the sign of the mode frequency. All simulations were run without toroidal rotation and toroidal rotation gradient.

Time (s)/V_{tor}	$k_y\rho_{ref}$	γ_{max}	ω
0.11/0	0.485	0.622	0.660
0.11/1	0.485	0.616	0.665
0.24/0	0.400	0.290	0.717
0.24/1	0.400	0.292	0.720
0.27/0	0.400	0.234	0.577
0.27/1	0.400	0.233	0.581
0.41/0	0.450	0.075	0.397
0.41/1	0.450	0.076	0.402

TABLE 3. The maximum growth rate and its corresponding mode frequency and $k_y\rho_{ref}$ in each simulation.

density points in figure 5 all appear between $0.2a$ and $0.3a$, thus there is a turbulent mode transition between $0.2a$ and $0.3a$ and the dominant turbulent modes are TEM at $0.3a$ and $0.4a$.

To investigate the effect of finite poloidal tilt on momentum transport in J-TEXT plasmas, $k_x\rho_{ref}$ was scanned while $k_y\rho_{ref}$ was selected as the value corresponding to the maximum growth rate, and the results are shown in figure 6. In GENE, the conversion between poloidal tilt angle θ and $k_x\rho_{ref}$ is as follows: $\theta = k_x\rho_{ref}/(s * k_y\rho_{ref})$, where s is magnetic shear. Similar to figure 4, toroidal rotation and toroidal rotation gradient have little effect on the growth rate/frequency spectra. The growth rate and mode frequency change slightly with θ. The standard output for momentum flux in GENE is calculated by taking moments of the distribution function with parallel velocity v_z,

https://doi.org/10.1017/S0022377820000343 Published online by Cambridge University Press

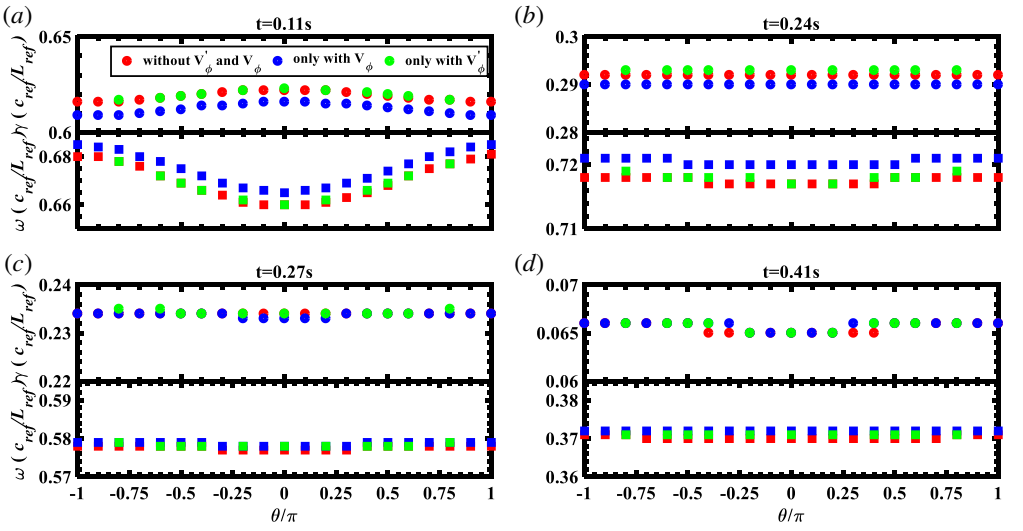

FIGURE 6. (*a–d*) Represent the relationship between growth rate/frequency and $k_x\rho_{\mathrm{ref}}$ at four electron density points at 0.2*a*. Red dots indicate that there is no rotation and rotation gradient, blue dots indicate that only rotation is added and green dots indicate that only a rotation gradient is added.

as an approximation of toroidal momentum flux. The toroidal momentum flux can be divided into three parts: diagonal term, pinch term and residual stress term

$$\Gamma_\phi^r = n_i m_i[-\chi_\phi V_\varphi' + V_p V_\varphi + C], \tag{3.1}$$

where n_i is ion density, m_i is ion mass, χ_ϕ is momentum diffusivity and V_p is convective velocity. In a linear simulation, the ion heat flux can be used to normalize the exponentially growing momentum flux (Camenen *et al.* 2011). The ion heat flux is defined as

$$Q_i^r = \frac{n_i T_i}{R_0}\chi_i R/L_{T_i}, \tag{3.2}$$

where χ_i is heat diffusivity and $L_{T_i} = -T_i/\nabla_r T_i$ is ion temperature characteristic length. The normalized ratio of toroidal momentum flux Γ_φ^r and heat flux Q_i^r can be written as

$$R_{\mathrm{nor}} = \frac{\Gamma_\phi^r}{Q_i^r} v_{\mathrm{ref}} = \frac{2}{R/L_{T_i}}\frac{\chi_\phi}{\chi_i}\frac{1}{v_{\mathrm{ref}}}\left[-R_0 V_\varphi' + \frac{R_0 V_p}{\chi_\phi}V_\varphi + \frac{R_0 C}{\chi_\phi}\right], \tag{3.3}$$

where $v_{\mathrm{ref}} = \sqrt{2\mathrm{T}_i/m_i}$ is the reference thermal velocity. Figure 7 shows the variation of the normalized ratio of toroidal momentum flux to heat flux with poloidal tilt angle θ at four density points at 0.2*a*. In figure 7, the normalized ratio R_{nor} is divided into a diagonal term, pinch term and residual stress term. The diagonal term is represented by circle dots, the pinch term is represented by diamond dots and the residual stress term is represented by square dots. As shown in figure 7, the diagonal term and pinch term change slightly with θ. The diagonal term is positive and the pinch term is negative at four density points at 0.2*a*. In GENE, the z direction is always defined to be parallel to the magnetic field. The toroidal momentum flux will therefore measure the flux of counter-clockwise momentum (viewed from above) for sign_Bt_CW $= -1$.

https://doi.org/10.1017/S0022377820000343 Published online by Cambridge University Press

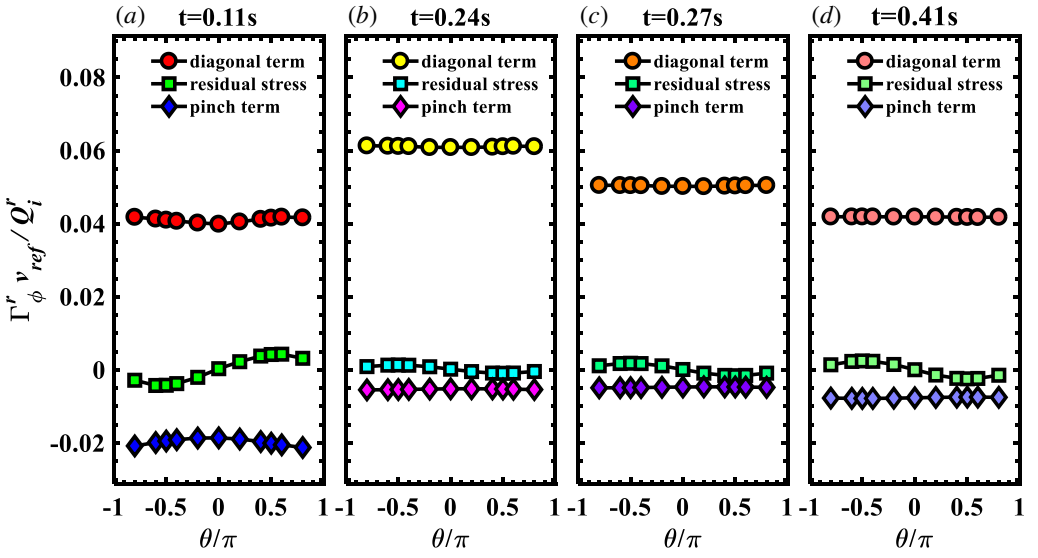

FIGURE 7. (*a–d*) Represent the relationship between the normalized ratio of toroidal momentum flux to heat flux and the poloidal tilt angle at four electron density points at 0.2*a*. Square dots indicate that there is no toroidal rotation and rotation gradient and represent the residual stress term. Circular dots represent the diagonal term and diamond dots represent the pinch term.

The momentum pinch term is always negative, which means the momentum pinch is inward and enhances the clockwise direction (counter-current direction in J-TEXT) rotation. This result is consistent with experimental results that the convective velocity is negative in toroidal rotation modulation experiments using a modulated electrode biasing in the J-TEXT tokamak (Liu *et al.* 2018). As the poloidal tilt angle θ is set to zero, the residual stress term is zero. The change trend of residual stress term with θ is periodic, and the sign of residual stress term depends on θ. The sign of poloidal tilt angle, which is related to the negative radial gradient of frequency $-\omega_r'$ can change at the TEM/ITG transition (Camenen *et al.* 2011). For ITG turbulence, $\omega_r > 0$ and $\omega_r' \propto -R/L_{T_i} < 0$, therefore the poloidal tilt angle is positive. For TEM turbulence, $\omega_r < 0$ and $\omega_r' > 0$ is mainly independent of R/L_{T_i}, so the poloidal tilt angle is negative. As the turbulent dominant modes at four density points are ITG, the poloidal tilt angle θ should be positive. As shown in figure 7, when θ is positive, the residual stress term is positive at the first time point, but the residual stress term becomes negative at the last three time points, which means the residual stress term reverses as the plasma density ramps up from 2.25×10^{19} m^{-3} to 3.46×10^{19} m^{-3}. For a counter-clockwise magnetic field, plasma current and positive magnetic shear, the residual stress term is radially outwards and therefore tends to enhance co-current core rotation at the first time point, and the residual stress term is radially inwards and therefore tends to enhance counter-current core rotation, which is consistent with the experimental phenomenon.

In formula (3.3) the normalized ratio of toroidal momentum flux and heat flux can be calculated by GENE, and the Prandtl number $P_r = \chi_\phi/\chi_i$, $R_0 V_p/\chi_\phi$ and $C_{\rm nor} = R_0 C/v_{\rm ref}\chi_\phi$ can be solved with three different sets of toroidal rotation V_φ and the toroidal rotation gradient V_φ'. Figure 8 shows the relationship between the Prandtl number P_r and the poloidal tilt angle at four electron density points at 0.2*a*, 0.3*a*

https://doi.org/10.1017/S0022377820000343 Published online by Cambridge University Press

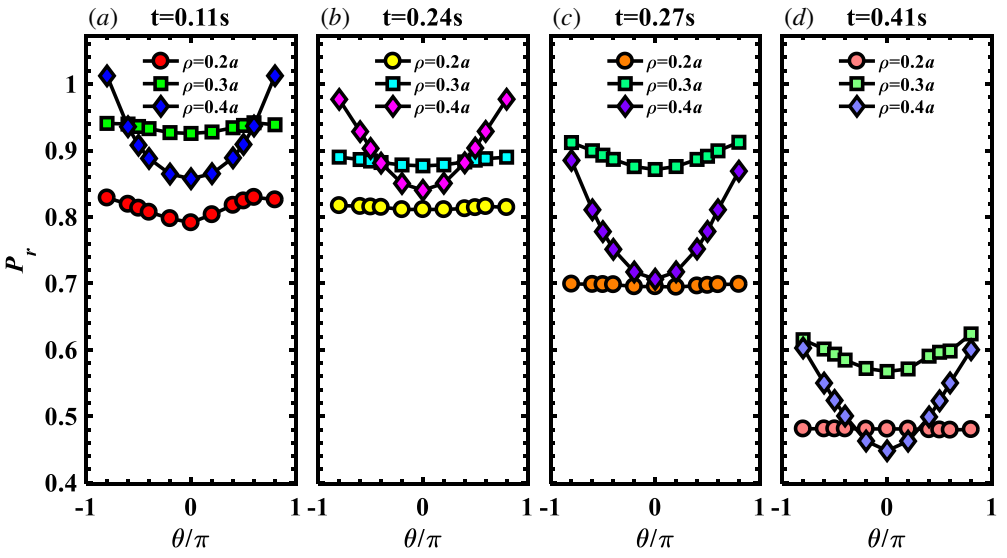

FIGURE 8. (*a–d*) Represent the relationship between the Prandtl number P_r and the poloidal tilt angle at four electron density points at 0.2a, 0.3a and 0.4a. Circular dots represent the Prandtl number at 0.2a, square dots represent the Prandtl number at 0.3a and diamond dots represent the Prandtl number at 0.4a.

and 0.4a. The Prandtl number changes slightly with the poloidal tilt angle at 0.2a and 0.3a, but the Prandtl number increases with the absolute value of the poloidal tilt angle at 0.4a. When the poloidal tilt angle is zero, the Prandtl number is the largest at 0.3a, and the Prandtl number increases first and then decreases at 0.2a to 0.4a at each density point. With the increase of the plasma density, the Prandtl number at each location gradually decreases from 1 to 0.4, when the poloidal tilt angle is zero. This trend is consistent with previous simulation results, although the decline is larger than the previous simulation results (Peeters *et al.* 2009). Due to the lack of experimental data on heat diffusivity, these simulation results cannot be compared with the J-TEXT experiment results. Figure 9 shows the relationship of the normalized ratio of convective velocity and momentum diffusivity R_0V_p/χ_ϕ with the poloidal tilt angle at four electron density points at 0.2a, 0.3a and 0.4a. Similar to the Prandtl number, R_0V_p/χ_ϕ changes slightly with the poloidal tilt angle at 0.2a and 0.3a, but R_0V_p/χ_ϕ increases with the absolute value of the poloidal tilt angle at 0.4a. When the poloidal tilt angle is zero, R_0V_p/χ_ϕ gradually decreases with the increase of the small radius at each density point. This trend is consistent with the experiment results in J-TEXT (Liu *et al.* 2018). The magnitude of R_0V_p/χ_ϕ is consistent with the theoretical analysis (Hahm *et al.* 2007); R_0V_p/χ_ϕ increases first and then decreases with the increase of the plasma density at each location when the poloidal tilt angle is zero. This trend is different from the previous simulation result that R_0V_p/χ_ϕ gradually increases when the normalized collisionality increases (Peeters *et al.* 2009). In figure 10, the relationship between the normalized residual stress related term $C_{\rm nor}$ and the poloidal tilt angle at four electron density points at 0.2a, 0.3a and 0.4a is shown. As the small radius increases, the maximum value of $C_{\rm nor}$ gradually increases at each density point. The maximum value of $C_{\rm nor}$ decreases first and then increases with the increase of the plasma density at each location. When the poloidal tilt angle is between -0.5 and 0.5, $C_{\rm nor}$ is approximately linear with the poloidal tilt angle

https://doi.org/10.1017/S0022377820000343 Published online by Cambridge University Press

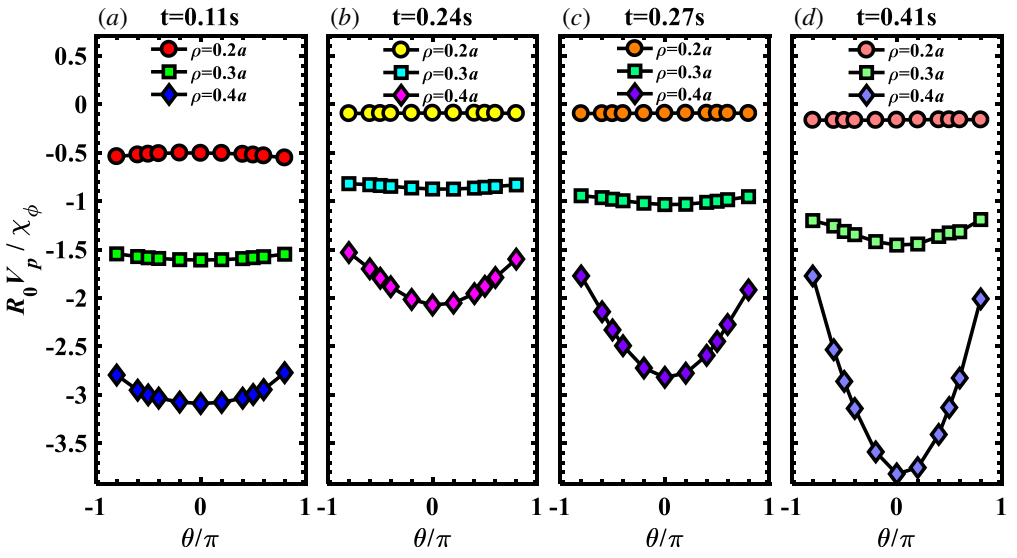

FIGURE 9. (*a–d*) Represent the relationship between the normalized ratio of convective velocity and momentum diffusivity R_0V_p/χ_ϕ and the poloidal tilt angle at four electron density points at 0.2*a*, 0.3*a* and 0.4*a*. Circular dots represent R_0V_p/χ_ϕ at 0.2*a*, square dots represent R_0V_p/χ_ϕ at 0.3*a* and diamond dots represent R_0V_p/χ_ϕ at 0.4*a*.

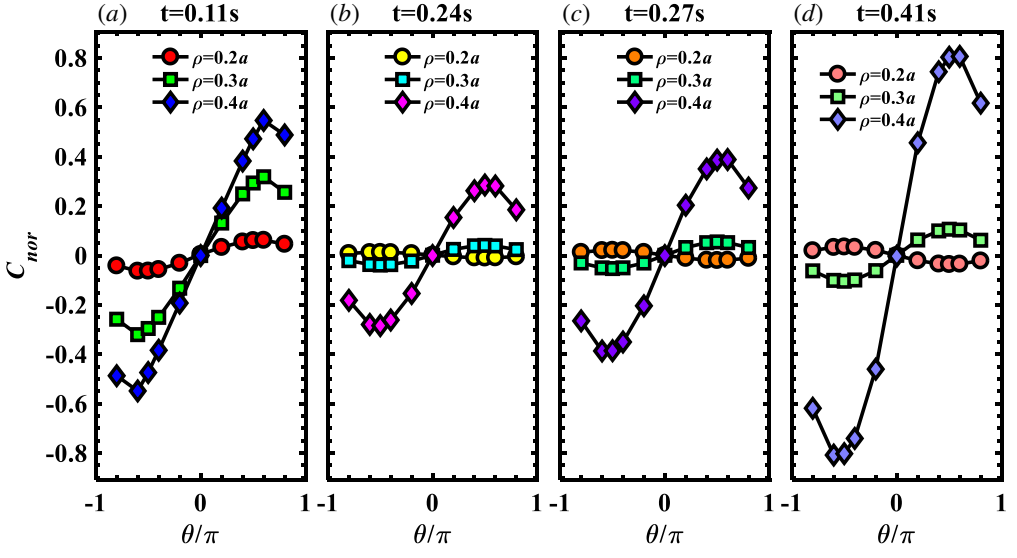

FIGURE 10. (*a–d*) Represent the relationship between the normalized residual stress related term $C_{\rm nor} = R_0C/v_{\rm ref}\chi_\phi$ and the poloidal tilt angle at four electron density points at 0.2*a*, 0.3*a* and 0.4*a*. Circular dots represent $C_{\rm nor}$ at 0.2*a*, square dots represent $C_{\rm nor}$ at 0.3*a* and diamond dots represent $C_{\rm nor}$ at 0.4*a*. $C_{\rm nor}$ at 0.2*a* is multiplied by 4.

at 0.4*a* which is consistent with the model used in AUG and KSTAR (McDermott *et al.* 2014; Angioni *et al.* 2017). The dominant turbulent modes are TEM at 0.3*a* and 0.4*a*, thus the poloidal tilt angles should be negative; $C_{\rm nor}$ is negative and enhances the counter-current rotation at each density point at 0.3*a* and 0.4*a*.

https://doi.org/10.1017/S0022377820000343 Published online by Cambridge University Press

4. Summary

The effect of finite poloidal tilt on momentum transport in core plasmas has been investigated using the local linear version of the gyrokinetic code GENE in the J-TEXT tokamak. During the plasma electron density ramp up, there is no change in the turbulent dominant mode, which is always ITG. However, the sign of the residual stress term changes from positive to negative when the plasma density exceeds a certain threshold when considering the poloidal tilt angle, which means the reverse of the residual stress term does not seem to be related to the change of the turbulent dominant mode. The pinch term is larger than the residual stress term at all four time points, which means the pinch term is always dominant in a J-TEXT core plasma. The positive residual stress term enhances co-current core rotation and the negative residual stress term enhance counter-current core rotation, which is consistent with the experimental phenomenon that the toroidal core rotation velocity increases toward the counter-current direction. All simulations in this paper are linear and a treatment of nonlinear effects is needed to confirm the results.

Acknowledgements

The authors are very grateful for the help of the J-TEXT team and GENE development team. This work was supported by the National Magnetic Confinement Fusion Science Program (nos 2015GB111002, 2015GB104000), by the China Postdoctoral Science Foundation (nos 2019M652651) and by the National Natural Science Foundation of China (nos 51821005, 71762031, 11575068, and 11905077).

REFERENCES

ANGIONI, C., CAMENEN, Y., CASSON, F. J., FABLE, E., MCDERMOTT, R. M., PEETERS, A. G. & RICE, J. E. 2012 Off-diagonal particle and toroidal momentum transport: a survey of experimental, theoretical and modelling aspects. *Nucl. Fusion* **52** (11), 114003.

ANGIONI, C. *et al.* 2017 A comprehensive study on rotation reversal in KSTAR: experimental observations and modelling. *Nucl. Fusion* **57** (12), 126008.

BARNES, M., PARRA, F. I., LEE, J. P., BELLI, E. A., NAVE, M. F. F. & WHITE, A. E. 2013 Intrinsic rotation driven by non-Maxwellian equilibria in Tokamak plasmas. *Phys. Rev. Lett.* **111** (5), 55005.

BERNARDO, J. *et al.* 2015 Density impact on toroidal rotation in Tore Supra: experimental observations and theoretical investigation. *Plasma Phys. Control. Fusion* **57** (3), 35002.

BONDESON, A. & WARD, D. J. 1994 Stabilization of external modes in tokamaks by resistive walls and plasma rotation. *Phys. Rev. Lett.* **72** (17), 2709–2712.

BUCHHOLZ, R., GROSSHAUSER, S. R., HORNSBY, W. A., MIGLIANO, P., PEETERS, A. G., CAMENEN, Y. & CASSON, F. J. 2014 Toroidal momentum transport in a tokamak due to profile shearing. *Phys. Plasmas* **12** (6), 62304.

BURRELL, K. H. *et al.* 1994 Role of the radial electric field in the transition from L (low) mode to H (high) mode to VH (very high) mode in the DIII-D tokamak*. *Phys. Plasmas* **1** (5), 1536–1544.

CAMENEN, Y., PEETERS, A. G., ANGIONI, C., CASSON, F. J. & HORNSBY, W. A. 2009 Transport of parallel momentum induced by current-symmetry breaking in toroidal plasmas. *Phys. Rev. Lett.* **102** (12), 125001.

CAMENEN, Y., IDOMURA, Y., JOLLIET, S. & PEETERS, A. G. 2011 Consequences of profile shearing on toroidal momentum transport. *Nucl. Fusion* **51** (7), 73039.

CARRARO, L., POL, G. D., PUIATTI, M. E., SATTIN, F., SCARIN, P. & VALISA, M. 2000 Edge temperature and density measurements with a thermal helium beam in the RFX reversed field pinch. *Plasma Phys. Control. Fusion* **42** (1), 1–14.

CASSON, F. J., PEETERS, A. G., CAMENEN, Y., HORNSBY, W. A. & SNODIN, A. P. 2009 Anomalous parallel momentum transport due to E×B flow shear in a tokamak plasma. *Phys. Plasmas* **16** (9), 92303.

CONNOR, J. W., HASTIE, R. J. & TAYLOR, J. B. 1979 High mode number stability of an axisymmetric toroidal plasma. *Proc. R. Soc. Lond.* A **365** (1720), 1–17.

DANNERT, T. & JENKO, F. 2005 Gyrokinetic simulation of collisionless trapped-electron mode turbulence. *Phys. Plasmas* **12** (7), 72309.

DEWAR, R. L. & GLASSER, A. H. 1983 Ballooning mode spectrum in general toroidal systems. *Phys. Fluids* **26** (10), 3038–3052.

DIAMOND, P. H. *et al.* 2013 An overview of intrinsic torque and momentum transport bifurcations in toroidal plasmas. *Nucl. Fusion* **53** (10), 104019.

DIAMOND, P. H., MCDEVITT, C. J., GÜRCAN, Ö.D., HAHM, T. S. & NAULIN, V. 2008 Transport of parallel momentum by collisionless drift wave turbulence. *Phys. Plasmas* **15** (1), 12303.

DUVAL, B. P., BORTOLON, A., KARPUSHOV, A., PITTS, R. A., POCHELON, A., SAUTER, O., SCARABOSIO, A., TURRI, G. & THE TCV TEAM 2008 Spontaneous L-mode plasma rotation scaling in the TCV tokamak. *Phys. Plasmas* **15** (5), 56113.

DUVAL, B. P., BORTOLON, A., KARPUSHOV, A., PITTS, R. A., POCHELON, A., SCARABOSIO, A. & THE TCV TEAM 2007 Bulk plasma rotation in the TCV tokamak in the absence of external momentum input. *Plasma Phys. Control. Fusion* **49** (12B), B195–B209.

GAROFALO, A. M. *et al.* 1999 Direct observation of the resistive wall mode in a tokamak and its interaction with plasma rotation. *Phys. Rev. Lett.* **82** (19), 3811–3814.

GENE DEVELOPMENT TEAM 2018 The Gyrokinetic Plasma Turbulence Code Gene: User Manual.

GÖRLER, T., LAPILLONNE, X., BRUNNER, S., DANNERT, T., JENKO, F., MERZ, F. & TOLD, D. 2011 The global version of the gyrokinetic turbulence code GENE. *J. Comput. Phys.* **230** (18), 7053–7071.

GÖRLER, T., TOLD, D., JENKO, F., HOLLAND, C., RHODES, T. L. & WHITE, A. E. 2014 A flux-matched gyrokinetic analysis of DIII-D L-mode turbulence. *Phys. Plasmas* **21** (12), 122307.

GÜRCAN, Ö. D., DIAMOND, P. H., HENNEQUIN, P., MCDEVITT, C. J., GARBET, X. & BOURDELLE, C. 2010 Residual parallel Reynolds stress due to turbulence intensity gradient in tokamak plasmas. *Phys. Plasmas* **17** (11), 112309.

HAHM, T. S. & BURRELL, K. H. 1995 Flow shear induced fluctuation suppression in finite aspect ratio shaped tokamak plasma. *Phys. Plasmas* **2** (5), 1648–1651.

HAHM, T. S., DIAMOND, P. H., GURCAN, O. D. & REWOLDT, G. 2007 Nonlinear gyrokinetic theory of toroidal momentum pinch. *Phys. Plasmas* **14** (7), 72302.

HILLESHEIM, J. C., PARRA, F. I., BARNES, M., CROCKER, N. A., MEYER, H., PEEBLES, W. A., SCANNELL, R., THORNTON, A. & THE MAST TEAM 2015 Dependence of intrinsic rotation reversals on collisionality in MAST. *Nucl. Fusion* **55** (3), 32003.

HORNSBY, W. A., ANGIONI, C., FABLE, E., MANAS, P., MCDERMOTT, R., PEETERS, A. G., BARNES, M., PARRA, F. & THE ASDEX UPGRADE TEAM 2017 On the effect of neoclassical flows on intrinsic momentum in ASDEX Upgrade Ohmic L-mode plasmas. *Nucl. Fusion* **57** (4), 46008.

HORNSBY, W. A., ANGIONI, C., LU, Z. X., FABLE, E., EROFEEV, I., MCDERMOTT, R., MEDVEDEVA, A., LEBSCHY, A., PEETERS, A. G. & THE ASDEX UPGRADE TEAM 2018 Global gyrokinetic simulations of intrinsic rotation in ASDEX Upgrade Ohmic L-mode plasmas. *Nucl. Fusion* **58** (5), 56008.

JENKO, F., DORLAND, W., KOTSCHENREUTHER, M. & ROGERS, B. N. 2000 Electron temperature gradient driven turbulence. *Phys. Plasmas* **7** (5), 1904–1910.

JENKO, F. & GENE DEVELOPMENT TEAM 2019 The GENE code. URL http://genecode.org.

LEE, W. D., RICE, J. E., MARMAR, E. S., GREENWALD, M. J., HUTCHINSON, I. H. & SNIPES, J. A. 2003 Observation of anomalous momentum transport in tokamak plasmas with no momentum input. *Phys. Rev. Lett.* **91** (20), 205003.

LIANG, Y. *et al.* 2019 Overview of the recent experimental research on the J-TEXT tokamak. *Nucl. Fusion* **59** (11), 112016.

https://doi.org/10.1017/S0022377820000343 Published online by Cambridge University Press

LIU, H., CHEN, Z., XU, Y., ZHU, L., CHEN, Z., ZHUANG, G. & THE J-TEXT TEAM 2018 Investigation of toroidal rotation modulation and momentum transport with electrode biasing in J-TEXT tokamak. *Plasma Phys. Control. Fusion* **60** (11), 115012.

LU, Z. X., WANG, W. X., DIAMOND, P. H., TYNAN, G., ETHIER, S., GAO, C. & RICE, J. 2015 Intrinsic torque reversals induced by magnetic shear effects on the turbulence spectrum in tokamak plasmas. *Phys. Plasmas* **22** (5), 55705.

MCDERMOTT, R. M. *et al.* 2011 Core momentum and particle transport studies in the ASDEX Upgrade tokamak. *Plasma Phys. Control. Fusion* **53** (12), 124013.

MCDERMOTT, R. M., ANGIONI, C., CONWAY, G. D., DUX, R., FABLE, E., FISCHER, R., PÜTTERICH, T., RYTER, F., VIEZZER, E. & THE ASDEX UPGRADE TEAM 2014 Core intrinsic rotation behaviour in ASDEX Upgrade ohmic L-mode plasmas. *Nucl. Fusion* **54** (4), 43009.

NA, D. H., NA, Y., LEE, S. G., ANGIONI, C. & YANG, S. M. 2016 Observation of the intrinsic rotation in KSTAR Ohmic L-mode plasmas. *Nucl. Fusion* **56** (3), 36011.

PARRA, F. I., BARNES, M. & PEETERS, A. G. 2011 Up-down symmetry of the turbulent transport of toroidal angular momentum in tokamaks. *Phys. Plasmas* **18** (6), 62501.

PEETERS, A. G., ANGIONI, C. & STRINTZI, D. 2007 Toroidal momentum pinch velocity due to the coriolis drift effect on small scale instabilities in a toroidal plasma. *Phys. Rev. Lett.* **98** (26), 265003.

PEETERS, A. G., ANGIONI, C., CAMENEN, Y., CASSON, F. J. & HORNSBY, W. A. 2009 The influence of the self-consistent mode structure on the Coriolis pinch effect. *Phys. Plasmas* **16** (6), 62311.

PEETERS, A. G. *et al.* 2011 Overview of toroidal momentum transport. *Nucl. Fusion* **51** (9), 94027.

RICE, J. E. *et al.* 2004 Observations of anomalous momentum transport in Alcator C-Mod plasmas with no momentum input. *Nucl. Fusion* **44** (3), 379–386.

RICE, J. E. *et al.* 2007 Inter-machine comparison of intrinsic toroidal rotation in tokamaks. *Nucl. Fusion* **47** (11), 1618–1624.

RICE, J. E. *et al.* 2011*a* Edge temperature gradient as intrinsic rotation drive in Alcator C-Mod tokamak plasmas. *Phys. Rev. Lett.* **106** (21), 215001.

RICE, J. E., DUVAL, B. P., REINKE, M. L., PODPALY, Y. A. & BORTOLON, A. 2011*b* Observations of core toroidal rotation reversals in Alcator C-Mod ohmic L-mode plasmas. *Nucl. Fusion* **51** (8), 83005.

RICE, J. E., MARMAR, E. S., BOMBARDA, F. & QU, L. 1997 X-ray observations of central toroidal rotation in ohmic Alcator C-Mod plasmas. *Nucl. Fusion* **37** (3), 421–426.

SCARABOSIO, A., BORTOLON, A., DUVAL, B. P., KARPUSHOV, A. & POCHELON, A. 2006 Toroidal plasma rotation in the TCV tokamak. *Plasma Phys. Control. Fusion* **48** (5), 663–683.

SHAING, K. C. & CRUME, E. J. 1989 Bifurcation theory of poloidal rotation in tokamaks: a model for L-H transition. *Phys. Rev. Lett.* **63** (21), 2369–2372.

SINGH, R., BRUNNER, S., GANESH, R. & JENKO, F. 2014 Finite ballooning angle effects on ion temperature gradient driven mode in gyrokinetic flux tube simulations. *Phys. Plasmas* **21** (3), 32115.

STOLTZFUS-DUECK, T. 2019 Intrinsic rotation in axisymmetric devices. *Plasma Phys. Control. Fusion* **61**, 12400312.

SUGAMA, H., WATANABE, T. H., NUNAMI, M. & NISHIMURA, S. 2011 Momentum balance and radial electric fields in axisymmetric and nonaxisymmetric toroidal plasmas. *Plasma Phys. Control. Fusion* **53** (2), 24004.

TERRY, P. W. 2000 Suppression of turbulence and transport by sheared flow. *Rev. Mod. Phys.* **72** (1), 109–165.

WALTZ, R. E., STAEBLER, G. M., CANDY, J. & HINTON, F. L. 2007 Gyrokinetic theory and simulation of angular momentum transport. *Phys. Plasmas* **14** (12), 122507.

WANG, L. & DIAMOND, P. H. 2013 Gyrokinetic theory of turbulent acceleration of parallel rotation in tokamak plasmas. *Phys. Rev. Lett.* **110** (26), 265006.

YAN, W. *et al.* 2018 Response of plasma rotation to resonant magnetic perturbations in J-TEXT tokamak. *Plasma Phys. Control. Fusion* **60** (3), 35007.

YAN, W., CHEN, Z. Y., JIN, W., HUANG, D. W., DING, Y. H., LI, J. C., ZHANG, X. Q., LEE, S. G., SHI, Y. J. & ZHUANG, G. 2014 Wavelength calibration of x-ray imaging crystal spectrometer on Joint Texas Experimental Tokamak. *Rev. Sci. Instrum.* **85** (11), 11E–416E.

ZHUANG, G., CHEN, J., LI, Q., GAO, L., WANG, Z. J., LIU, Y. & CHEN, W. 2013 First results of the J-TEXT high-resolution 3-wave polarimeter-interferometer system. *J. Instrum.* **8** (10), C10019.